Supporting Information

Three Zr(IV)-Substituted Polyoxotungstate Aggregates: Structural Transformation from Tungstoantimonate to Tungstophosphate Induced by pH

Hai-Lou Li, Chen Lian, Da-Peng Yin and Guo-Yu Yang*

MOE Key Laboratory of Cluster Science, School of Chemistry and Chemical Engineering, Beijing Institute of Technology, Beijing 102488

Table S1. Bond valence sum (BVS) calculations of all W, P, Sb and Zr atoms in **1.**

Table S2. Bond valence sum (BVS) calculations of all W, P, Sb and Zr atoms in **2.**

Table S3. Bond valence sum (BVS) calculations of all W, P, Sb and Zr atoms in **3.**

Materials and methods. The trivacant precursor $Na_9[B\text{-}\alpha\text{-}SbW_9O_{33}]\cdot 19.5H_2O$ was obtained as previously described[1] and further identified by IR spectroscopy. All other chemicals were commercially purchased and used without further purification. IR spectra were recorded with a Nicolet 170 SXFT−IR spectrometer using KBr pellets in the range of 400–4000 cm^{-1}. Powder X-ray diffraction (PXRD) patterns were obtained by using a Bruker D8 Advance XRD diffractometer with Cu Kα radiation (λ = 1.54056 Å). Thermogravimetric (TG) analyses were performed under a N_2 atmosphere on a Mettler–Toledo TGA/SDTA 851e instrument with a heating rate of 10 °C min^{-1} from 25 to 500 °C. GC were carried out with a Varian 430-GC gas chromatograph. GC-MS were obtained from a Varian 450-GC/240-MS gas chromatograph-mass spectrometer.

[1] Bösing, M.; Loose, I.; Pohlmann, H.; Krebs, B. New Strategies for the Generation of Large Heteropolymetalate Clusters: The β-B-SbW_9 Fragment as a Multifunctional Unit. *Chem. Eur. J.* **1997**, 3, 1232-1237.

X-ray Crystallography. Suitable crystals of **1**, **2** and **3** were picked up from the mother liquors and sealed to a glass tube closed at both ends. Intensity data were collected on a Gemini A Ultra diffractometer equipped with graphite monochromated Mo Kα (λ = 0.71073 Å) at 293(2) K. The program SADABS was used for the absorption correction. The structures were solved by the direct method and refined on F^2 by full-matrix least-squares methods using the SHELX 97 program package.[2,3] No hydrogen atoms associated with water molecules were located from the difference Fourier map. In the structural refinements, the "omit" constraint was used owing to the low-quality diffraction data in high θ. To balance the charge, **1**, **2** and **3** should be added with 2, 12, 9 protons respectively. In the refinements, 9, 14 and 53 lattice water molecules for **1**, **2** and **3** were found from the Fourier maps. The crystallographic data and structure refinement parameters for **1**, **2** and **3** were listed in Table 1. CCDC reference no. 1882473-1882475 for **1**–**3**.

[2] Sheldrick, G. M. SHELXL 97, Program for Crystal Structure Refinement; University of Göttingen: Göttingen, Germany, 1997.

[3] Sheldrick, G. M. SHELXS 97, Program for Crystal Structure Solution; University of Göttingen: Göttingen, Germany, 1997.

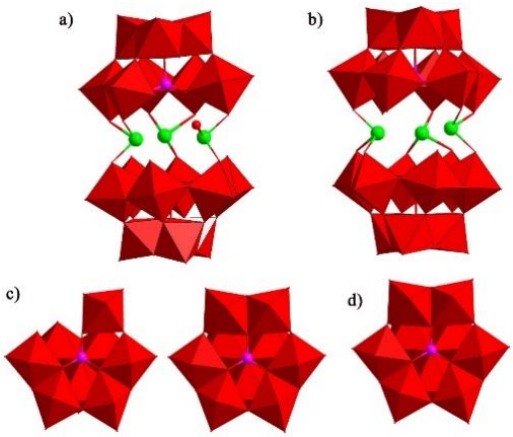

Figure S1. a) The structure of $[Sb_3(PW_8O_{32})(PW_9O_{34})]^{11-}$ in **2**; b) The structure of $[Sb_3(SiW_9O_{34})_2]^{11-}$ in **5**; c) The $\{PW_8\}$ segment and $\{PW_9\}$ segment; d) The $\{SiW_9\}$ fragment.

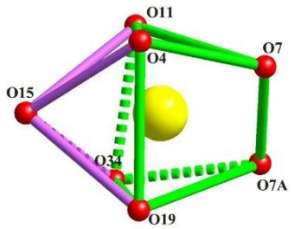

Figure S2. The hepta-coordinate monocapped trigonal prism geometry of the ZrO_7 group in **2.**

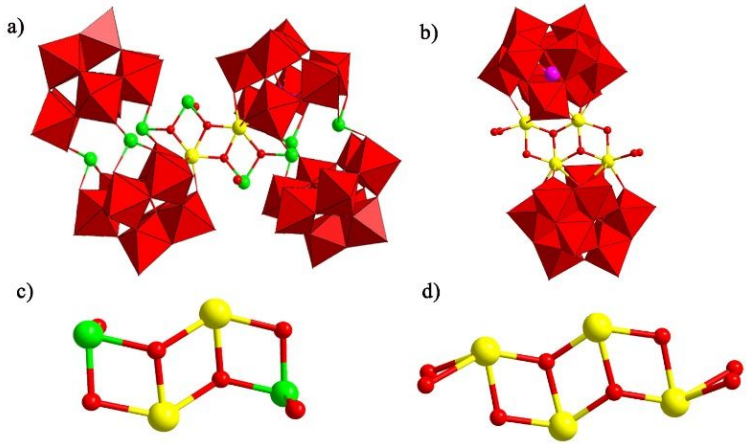

Figure S3. a) The structure of **2**; b) The structure of **6**; c) The tetranuclear heterometallic $[Sb_2Zr_2(OH)_2O_4]^{4+}$ cluster; d) The tetranuclear $[Zr_4O_2(OH)_2(H_2O)_4]^{10+}$ cluster.

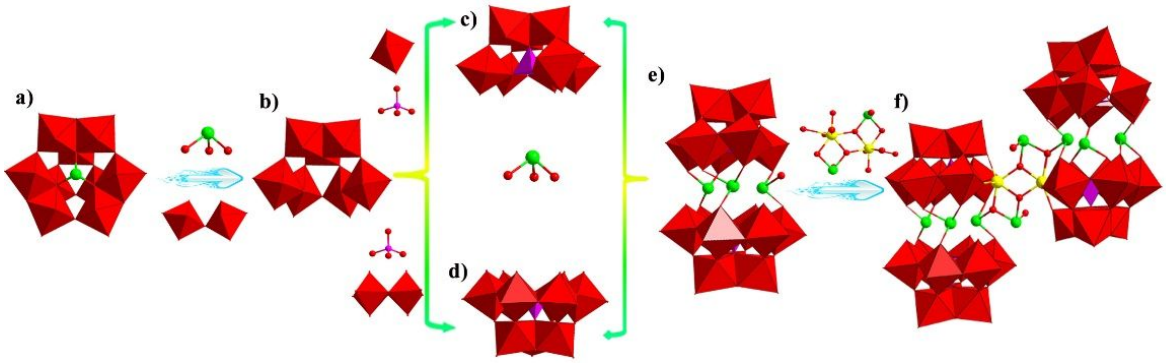

Figure S4. Evolution from $\{SbW_9\}$ to compound **2**. a) The $\{SbW_9\}$ precursor; b) The W_7O_{28} intermediate; c) The $\{PW_8\}$ segment; d) The $\{PW_9\}$ segment; e) The $[Sb_3(PW_8O_{32})(PW_9O_{34})]^{11-}$ cluster; f) The structure of **2.**

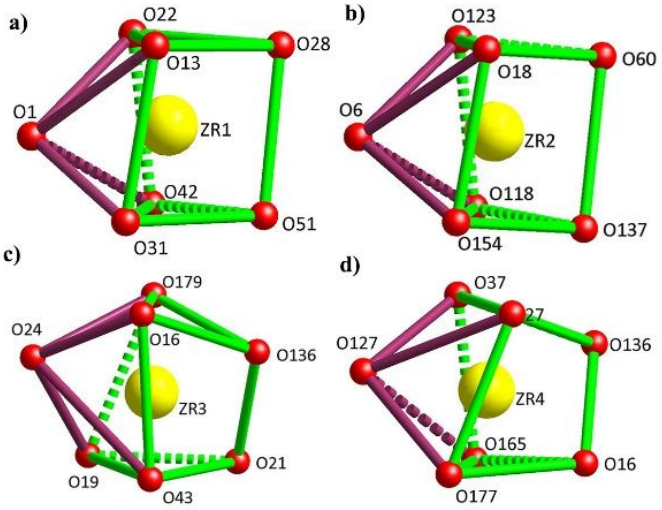

Figure S5. a~d) The hepta-coordinate monocapped trigonal prism geometry of the $Zr1^{4+}$, $Zr2^{4+}$, $Zr3^{4+}$ and $Zr4^{4+}$ in **3**.

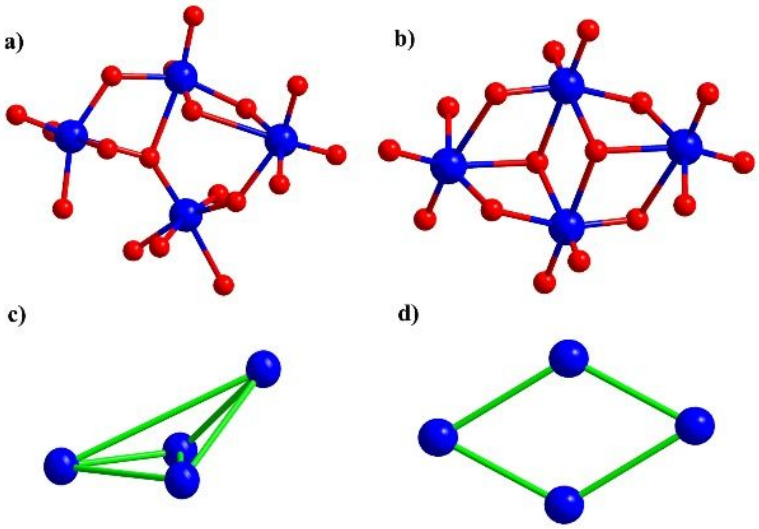

Figure S6. a) The W_4O_{18} fragment in **3**; b) The W_4O_{16} fragment in **7**; c) The tilted trigonal pyramid geometry; d) The rhombus geometry.

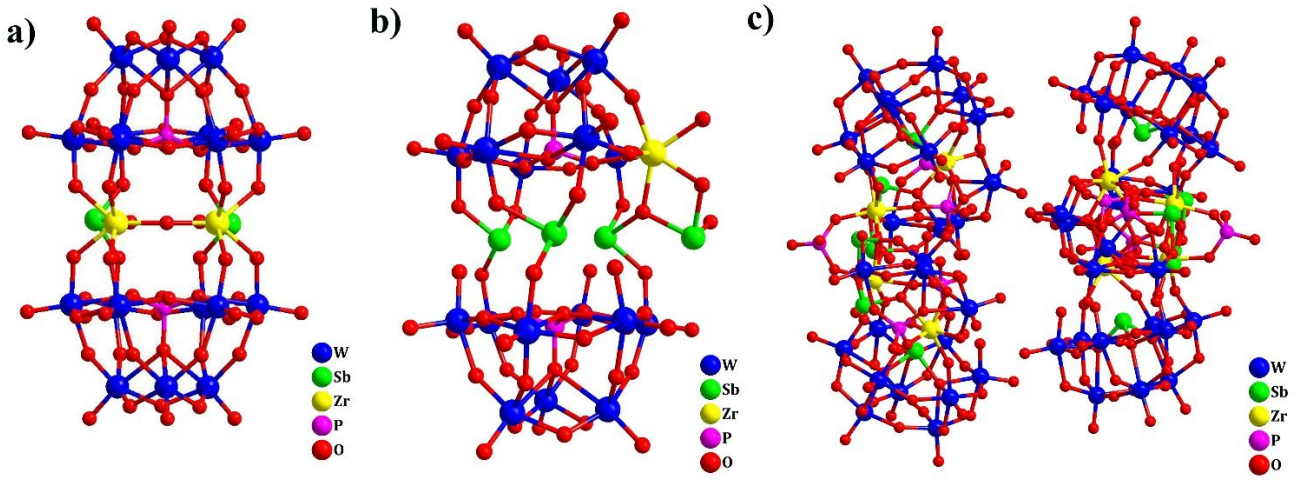

Figure S7. a), b) and c) The asymmetric structural units of **1**, **2** and **3**.

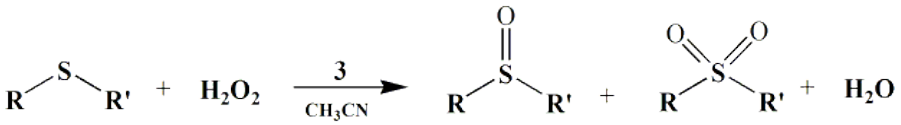

Scheme S1. Catalytic oxidation of thioethers.

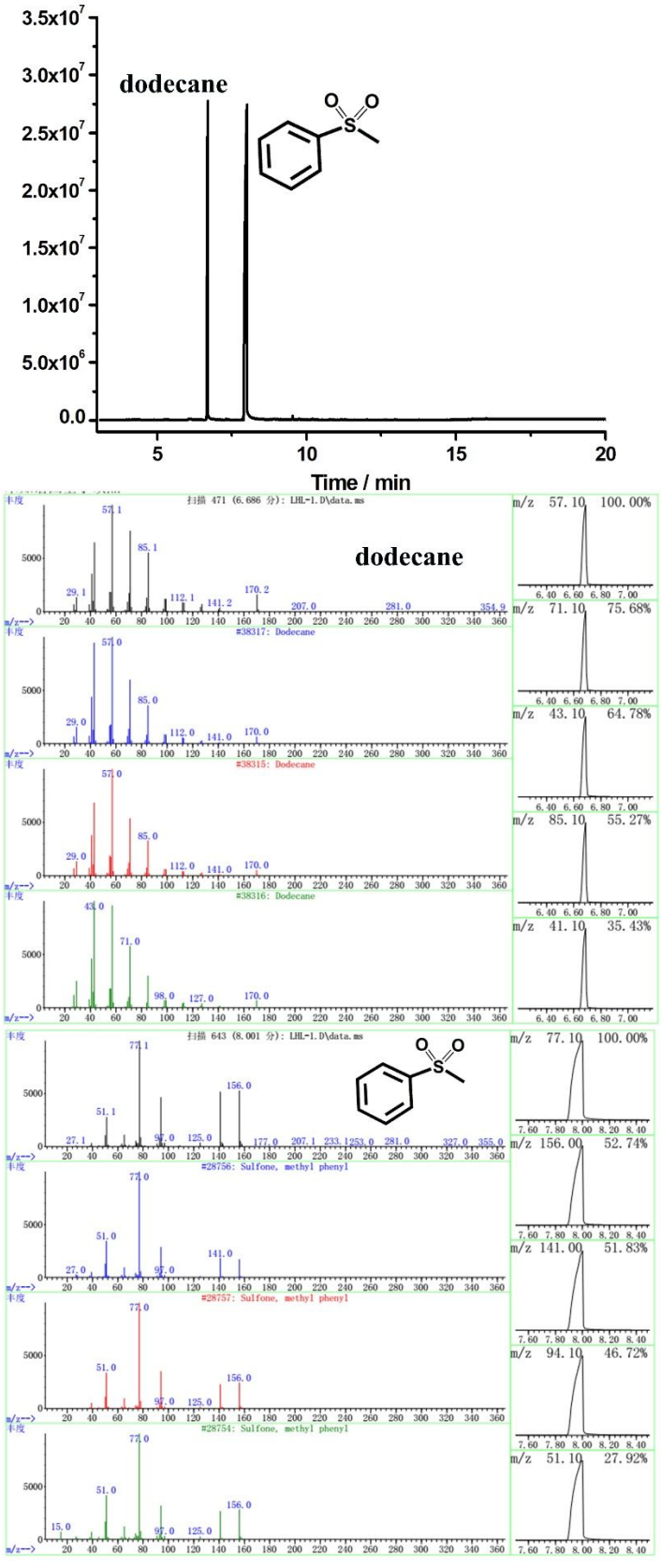

Figure S8. MS spectra for the products of MPS and dodecane and GC trace of the catalytic results for the $MPSO_2$. Reactions conditions: MPS (0.5 mmol), 1000 S/C and 2.4 O/S in CH_3CN (3 mL) at 45 °C, 60 min.

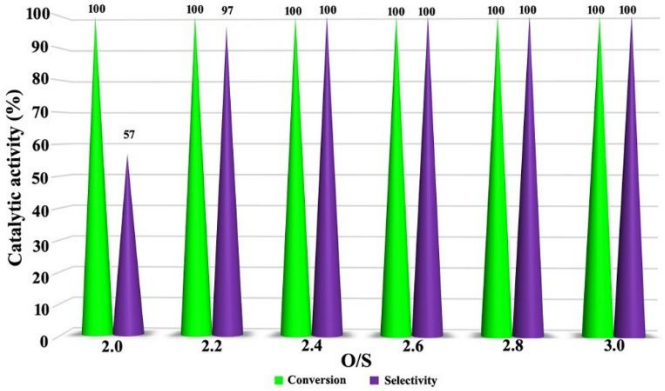

Figure S9. The conversion of DPS and selectivity of $DPSO_2$ with different amount of oxidant under the reaction conditions: 0.5 mmol substrate, 1000 S/C molar ratio, 3 mL acetonitrile, at 60 °C, 1h.

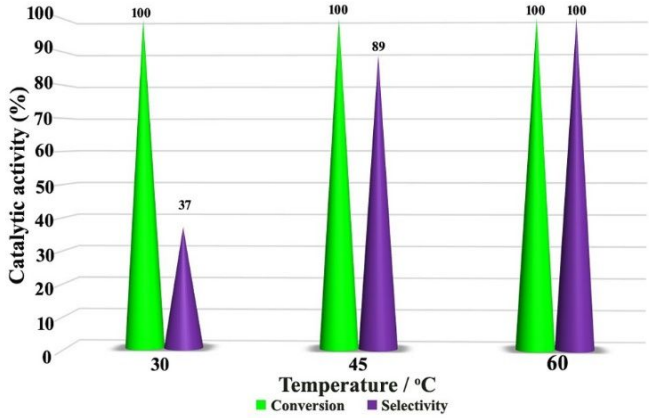

Figure S10. The conversion of DPS and the selectivity of $DPSO_2$ at different temperatures under the reaction conditions: 0.5 mmol substrate, 2.4 O/S molar ratio, 1000 S/C molar ratio, 3 mL acetonitrile, 1h.

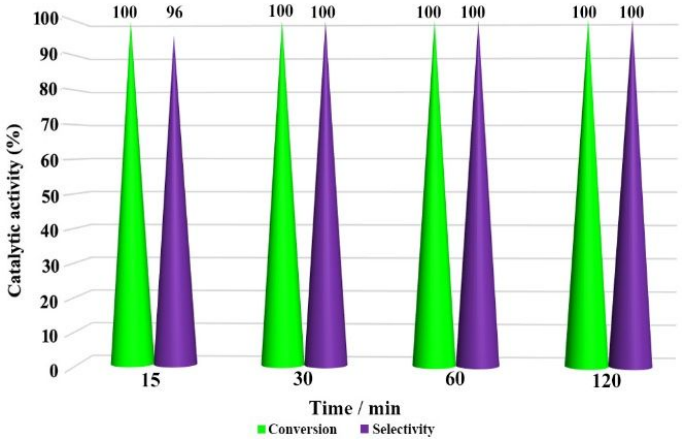

Figure S11. The conversion of DPS and the selectivity of $DPSO_2$ at different reaction time under the reaction conditions: 0.5 mmol substrate, 2.4 O/S molar ratio, 1000 S/C molar ratio, 3 mL acetonitrile, at 60°C.

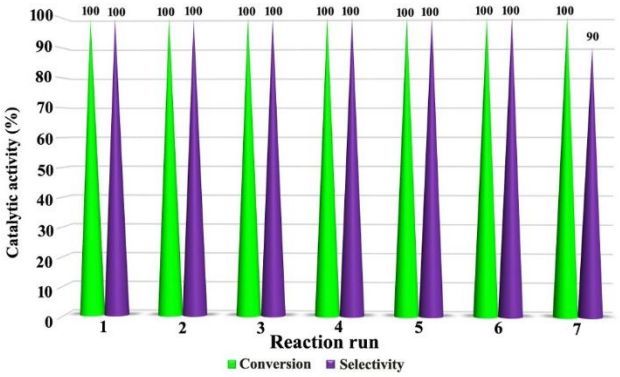

Figure S12. Recycling of the catalytic system for the oxidation of DPS at 60°C, 2.4 O/S molar ratio, 30 min.

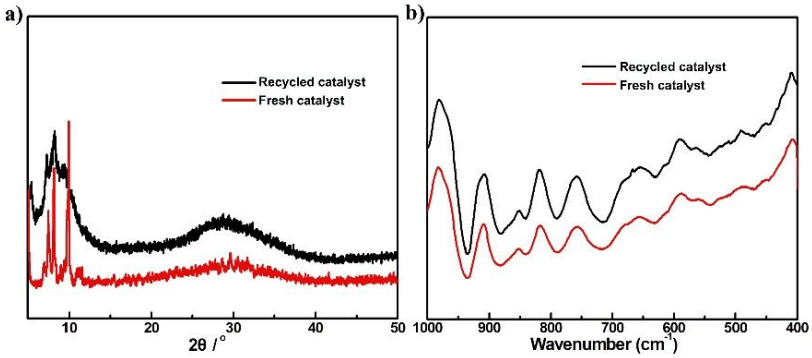

Figure S13. PXRD patterns and IR spectra of catalyst before and after the catalytic reaction.

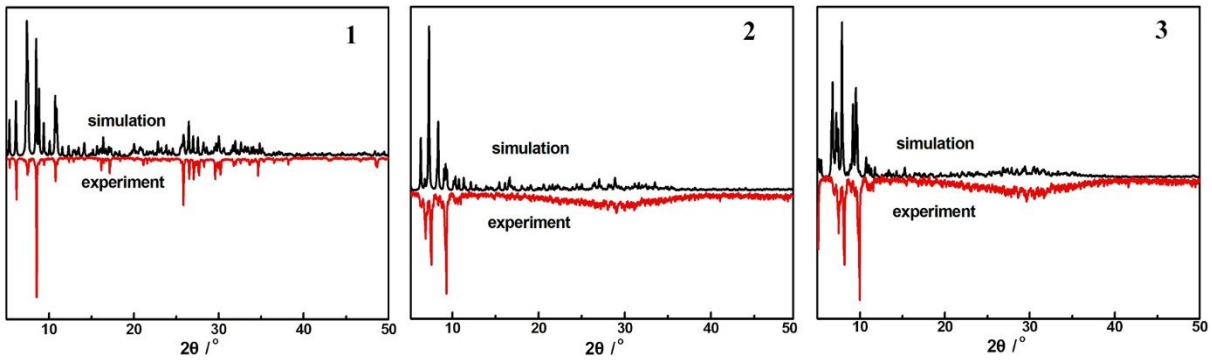

Figure S14. The experimental and simulated PXRD patterns of **1**, **2** and **3**.

As shown in Figure S14, the experimental powder x-ray diffraction (PXRD) patterns agree well with the single crystal X-ray diffraction simulation patterns, indicating that the samples of **1**, **2** and **3** are pure phase. The slight difference between the experimental and the simulated patterns may be due to the change in the preferred orientation of the powder samples during the acquisition of the experimental PXRD patterns.

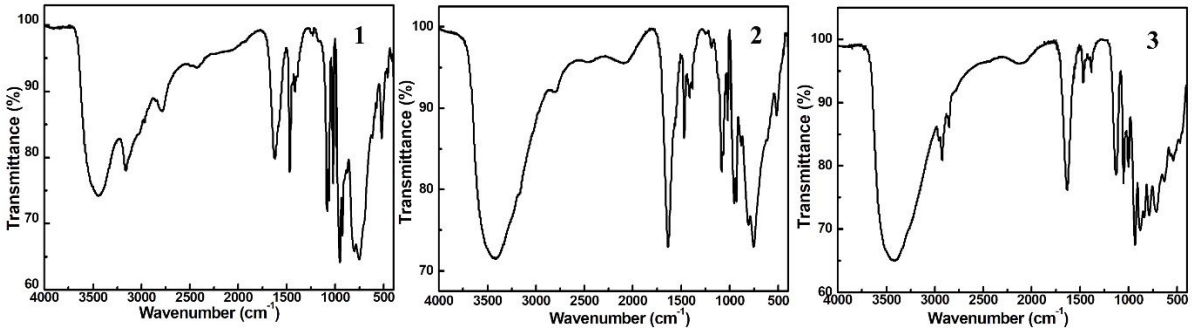

Figure S15. IR spectra of **1, 2** and **3**.

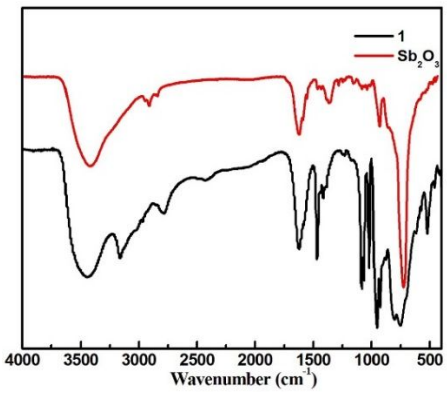

Figure S16. IR spectra of **1** and Sb_2O_3.

IR spectra of **1**–**3** have been recorded on a Nicolet 170 SXFT−IR spectrometer by utilizing KBr pellets in the range of 4000–400 cm^{-1} (Figure S15). It is well-known that the broad vibration band located in the range of 3410−3443 cm^{-1} for **1**–**3** is indicative of the presence of lattice or coordination water molecules. Three weak bands appearing at 2978–3166 cm^{-1}, 2789–2801 cm^{-1} and 1462–1466 cm^{-1} are respectively assigned to the N–H, C–H and C–N stretching vibrations,[4] illustrating the presence of dimethylamine components. In the low-wavenumber region, IR spectra of **1**, **2** and **3** display the characteristic vibration patterns derived from the polyoxotungstate skeleton. Two sharp absorption peaks centered at 1095–1034 cm^{-1} in **1** are ascribed to the $\nu_{(P-O)}$ stretching vibration. In addition, the IR spectrum of **1** shows three W–O characteristic vibration bands attributable to $\nu_{(W-Ot)}$, $\nu_{(W-Ob)}$ and $\nu_{(W-Oc)}$ observed at 961, 821, and 750 cm^{-1}, respectively. In order to find the corresponding vibration $\nu_{(Sb-O)}$ accurately, the IR spectrum of Sb_2O_3 has been performed under the same conditions (Figure S16). It's easy to see that the 714 cm^{-1} vibration band in **1** attributes to $\nu_{(Sb-O)}$. Similarly, in the IR spectrum of **2**, two sharp absorption peaks centered at 1089–1028 cm^{-1} are ascribed to the $\nu_{(P-O)}$ stretching vibration, three W-O characteristic vibration bands assigned to $\nu_{(W-Ot)}$, $\nu_{(W-Ob)}$, $\nu_{(W-Oc)}$ and $\nu_{(Sb-O)}$ locate at 945, 826, 762 and 708 cm^{-1}. Likewise, the IR spectrum of **3** shows two bands attributable to $\nu_{(P-O)}$ centring at 1066 cm^{-1} and 1004 cm^{-1}. Differently, four characteristic vibrational bands of $\nu_{(W-Ot)}$, $\nu_{(W-Ob)}$, $\nu_{(W-Oc)}$ and $\nu_{(Sb-O)}$[5,6] originating from the trivacant Keggin $[SbW_9O_{33}]^{9-}$ framework are observed at 937, 881, 779, and 719 cm^{-1}, respectively.

[4] Li, H. L.; Yang, W.; Wang, X. H.; Chen, L. J.; Ma, J. R.; Zheng, L. W.; Zhao, J. W. Self-Assembly of a Family of Isopolytungstates Induced by the Synergistic Effect of the Nature of Lanthanoids and the pH Variation in the Reaction Process: Syntheses, Structures, and Properties. *Cryst. Growth Des.* **2016**, *16*, 108-120.

[5] Gupta, R.; Saini, M. K.; Doungmene, F.; Oliveira, P.; Hussain, F. Lanthanoid containing phosphotungstates: the syntheses, crystal structure, electrochemistry, photoluminescence and magnetic properties. *Dalton Trans*. **2014**, *43*, 8290-8299.

[6] Zhao, J.-W.; Cao, J.; Li, Y.-Z.; Zhang, J.; Chen, L.-J. First Tungstoantimonate-Based Transition-Metal–Lanthanide Heterometallic Hybrids Functionalized by Amino Acid Ligands. *Cryst. Growth Des.* **2014**, *14*, 6217-6229.

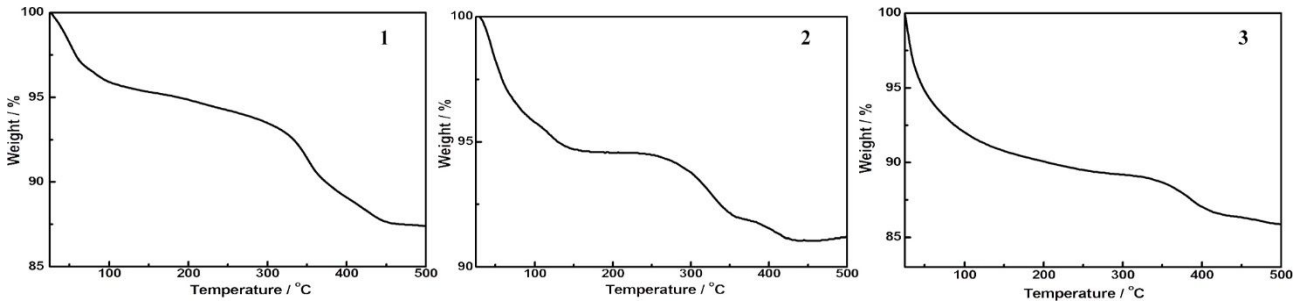

Figure S17. The TG curves of **1**, **2** and **3**.

In order to examine the thermal stability and determine the number of lattice water molecules and free dimethylamine cations of **1**, **2** and **3**, TG analyses have been investigated on the samples under the flowing N_2 atmosphere with a heating rate of 10 °C/min in the temperature range of 25–500 °C (Figure S17). The TG curves of **1**–**3** show the two-step weight loss process. The first step of

5.04% (calcd. 5.17%) for **1** occurs between 25 and 200 °C, which is attributable to the loss of sixteen lattice water molecules; 5.34% (calcd. 5.59%) for **2** approximately corresponds to the liberation of thirty-three lattice water molecules; and 10.08% (calcd. 10.19%) for **3** results from the releasing of fifty-three lattice water molecules. The second step occurs between 200 and 500 °C. The weight loss of 7.59% (calcd. 7.11%) corresponds to the removal of seven dimethylamine molecules and the dehydration of nine protons for **1**. The weight loss of 3.75% (calcd. 4.24%) is belonging to the removal of six dimethylamine molecules and the dehydration of eighteen protons and two hydroxyls for **2**. The weight loss of 3.66% (calcd. 3.22%) is due to the removal of four dimethylamine molecules and the dehydration of eight point five protons and five hydroxyls for **3**.

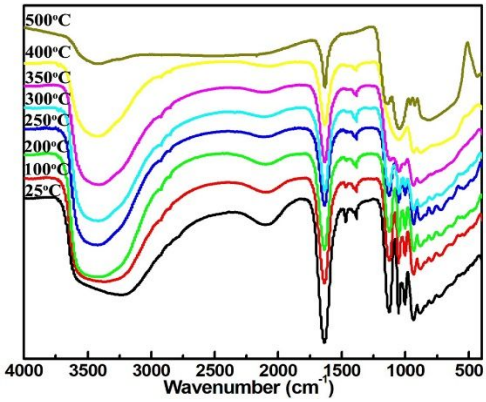

Figure S18. The IR spectra of **3** at different temperatures.

Thermal stability Studies. In order to further understand the thermal decomposition process, **3** as representative has been studied by means of IR spectra. According to the TG curve, the sample has been measured ranging from 25 to 500 °C (Figure S17). As show in Figure S18, when the temperature up to 250 °C, the structure of **3** almost remains unchanged in spite of the release of some lattice water molecules. When reaching 350 °C, it can be very easily seen that the characteristic peaks of POM slightly weaken and the stretching vibration peaks of N–H, C–H and C–N are almost disappeared, indicating that although releasing all lattice water molecules and some small organic molecule components, the polyoxoanionic skeleton is still maintained. Rising to 400 °C, the characteristic peaks of POM slightly change, suggesting that the subject POM skeleton still exists. Obviously, the characteristic peaks of **3** are prominently changed upon 500 °C, indicating the collapse of structure skeleton.

Table S1. Bond valence sum (BVS) calculations of all W, P, Sb and Zr atoms in **1**.

Atom	BVS
W	6.084-6.327
P	4.993-5.103
Sb	3.089-3.111
Zr	3.779-3.838

Table S2. Bond valence sum (BVS) calculations of all W, P, Sb and Zr atoms in **2**.

Atom	BVS
W	6.060-6.472
P	5.131-5.171
Sb	2.515-2.930

Zr	4.124

Table S3. Bond valence sum (BVS) calculations of all W, P, Sb and Zr atoms in **3**.

Atom	BVS
W	5.668-6.596
P	4.679-5.320
Sb	2.575-3.085
Zr	3.915-4.262